JCTC Journal of Chemical Theory and Computation

Active Role of Hydrogen Bonds in Rupe and Meyer−Schuster Rearrangements

Shinichi Yamabe, Noriko Tsuchida, and Shoko Yamazaki*

Department of Chemistry, Nara University of Education, Takabatake-cho, Nara 630-8528, Japan

Received April 10, 2006

Abstract: Rupe and Meyer−Schuster rearrangements for the $R_2C(OH)-C\equiv C-H + H_3O^+$ and $(H_2O)_9$ model (R = methyl and phenyl groups) have been investigated by the use of density functional theory calculations. In the substrate $R_2C(OH)-C\equiv CH$ catalyzed by $H_3O^+(H_2O)$, three reaction channels, the two rearrangements and S_N (nucleophilic substitution), were predicted by the frontier molecular orbital theory. The S_N (the OH-group exchange) path was found to have a large activation energy. For 2-methylbut-3-yn-2-ol (R = Me), the Rupe rearrangement has been found to be much more favorable than the Meyer−Schuster rearrangement. For 1,1-diphenylprop-2-yn-1-ol (R = Ph), the occurrence of Meyer−Schuster rearrangement is very likely with the small activation energy. Both rearrangements do not involve the carbonium ion intermediates. However, the calculated geometries of the first transition state are carbonium-ion-like. Dehydration and hydration may occur via the intermolecular proton relay along the hydrogen-bond chains. Minimal models were proposed to represent reaction mechanisms of both rearrangements.

I. Introduction

The Rupe rearrangement is the acid-catalyzed rearrangement of tertiary α-acetylenic alcohols (propargylic alcohols) leading to the formation of α,*β*-unsaturated ketones.[1] The Meyer−Schuster rearrangement is the 1,3-shift isomerization of secondary and tertiary α-acetylenic alcohols to ketones or aldehydes.[2,3] The two rearrangements are shown in Schemes 1 and 2, respectively.

It is now agreed that the Rupe rearrangement proceeds through a dehydration−hydration sequence with enyne intermediates. These intermediates were sometimes isolated.[4] When a C−H bond adjacent to the C−OH bond is present, the Rupe rearrangement takes place. When a C−H bond adjacent to the C−OH is absent, the Meyer−Schuster rearrangement occurs. In both rearrangements, carbonium ions are thought to be involved. This is because the dehydration in the first step gives the tertiary carbon atom with the acetylene substituent for the enhanced delocalization of the cation charge. The mechanism of the Meyer−Schuster rearrangement of tertiary arylpropargyl alcohols to α,*β*-carbonyl compounds was studied kinetically.[5] Two transition-state models were suggested (Scheme 3).

Scheme 1. Mechanism of the Rupe Rearrangement Generally Considered So Far

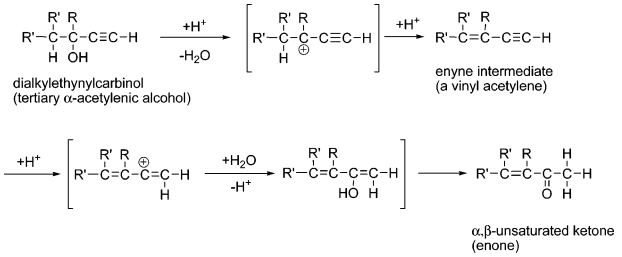

The synthetic utility of the two classic rearrangements is well-established. The Rupe rearrangement was utilized for the synthesis of tricyclic skeletons such as (±)-capnellene[6] and cyathins.[7] The rearrangement was also used for the large-scale synthesis of unsaturated ketones from steroidal propargylic alcohols.[8] The Meyer−Schuster rearrangement was used as key steps for syntheses of a histamine H_3-receptor antagonist[9] and an antifungal mold metabolite.[10] The re-

* Author to whom correspondence should be addressed. Fax: +81-742-27-9289. E-mail: yamazaks@nara-edu.ac.jp.

10.1021/ct600132k CCC: $33.50 © 2006 American Chemical Society
Published on Web 07/22/2006

Scheme 2. Mechanism of the Meyer−Schuster Rearrangement Generally Considered So Far

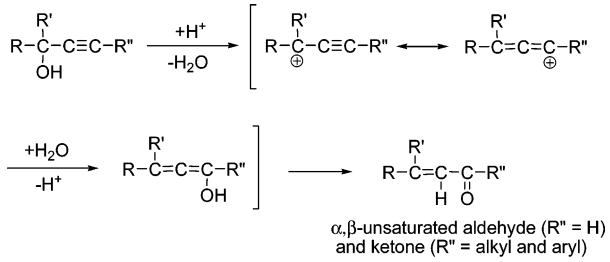

Scheme 3. Transition-State Models for the Meyer−Schuster Rearrangement

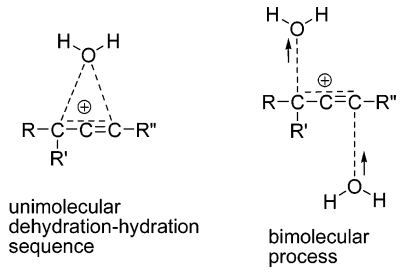

arrangement was also applied to the synthesis of α,*β*-unsaturated thioesters.[11] Both rearrangements were investigated in water at high temperatures (200−290 °C), and it was shown that an elevated temperature without acids is effective.[12] Furthermore, recently, various metal-catalyzed Rupe and Meyer−Schuster rearrangements were reported.[13] In addition, to suppress Rupe and Meyer−Schuster rearrangements is an important task for some C−C bond formation reactions involving propargyl alcohols.[14]

On the other hand, their precise mechanisms are still open to question. Tapia et al. carried out computational studies of the Meyer−Schuster rearrangement.[15] However, their models were too small or inappropriate to describe the dehydration−hydration sequence. For instance, a propargylic alcohol substrate, $Me_2C(OH)$−C≡CH, was employed in a combined quantum-chemical/Monte Carlo study.[15a] However, the substrate with the C−H bond should undergo not the Meyer−Schuster but the Rupe rearrangement. Except for those of Tapia et al., there have been no computational studies. To elucidate the entire process and the driving force of both rearrangements, we conducted a computational study on the reacting system, $R_2C(OH)$−C≡C−H + H_3O^+ + $(H_2O)_9$ (R = Me and Ph). Particular interest lies both in the role of hydrogen bonds to control the (de)hydration and in the intermediacy of the carbonium ions, exhibited in brackets in Schemes 1 and 2. The reacting systems of both rearrangements are composed of only C, H, and O atoms, which are fundamental elements of organic compounds. Elucidation of their mechanisms is expected to give deep insight into other acid-catalyzed solvolytic reactions.

II. Method of Calculations

The geometries of the reacting system starting from $R_2C(OH)$−C≡C−H + $H_3O^+(H_2O)_9$ were determined by density functional theory calculations. The B3LYP method[16] was used. B3LYP seems to be a suitable method, because it includes the electron correlation effect to some extent. The basis set employed is 6-31G*. Then, the geometry optimizations were carried out by RB3LYP/ 6-31G*.

Transition states (TSs) were characterized by vibrational analysis, which checked whether the obtained geometries have single imaginary frequencies ($\nu^{\ddagger}$). From TSs, reaction paths were traced by the intrinsic reaction coordinate method[17] to obtain the energy-minimum geometries. Relative electronic (and Gibbs free) energies were refined by single-point calculations of RB3LYP/6-311+G(d,p) [self-consistent reaction field (SCRF) = dipole, solvent = water][18] on the RB3LYP/6-31G* geometries and its zero-point vibrational [and thermal correction (T = 300 K, P = 1 atm)] energies (ZPEs).

All of the calculations were carried out using the Gaussian 03[19] program package installed on a Compaq ES 40 at the Information Processing Center (Nara University of Education).

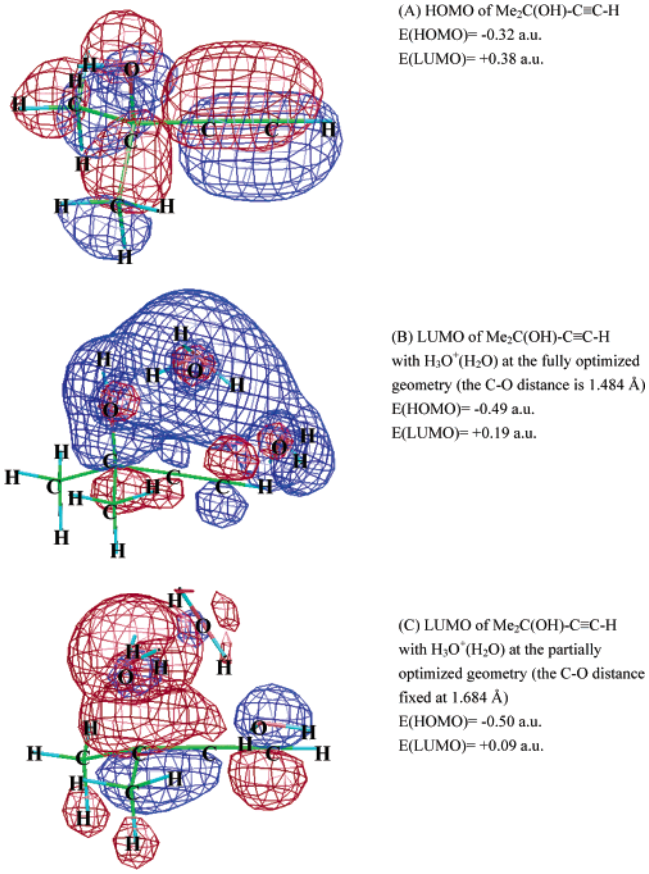

Figure 1. Shapes of frontier orbitals; HOMO and LUMO of the $Me_2C(OH)$−C≡C−H substrate without (A) and with the $H_3O^+(H_2O)$ catalyst (B) and (C). *E*(HOMO) and *E*(LUMO) are orbital energies computed by RHF/STO-3G.

III. Results and Discussions

Frontier Molecular Orbital Analysis of 2-Methylbut-3-yn-2-ol, $Me_2C(OH)$−C≡C−H. The substrate, $Me_2C(OH)$−C≡C−H, has two nucleophilic sites, the O−H oxygen lone pair and the triple bond. Figure 1A shows its highest occupied molecular orbital (HOMO) shape. An acid catalyst, $H_3O^+(H_2O)$, may be bound to those sites. That is, the HOMO of the substrate may overlap effectively with the lowest vacant

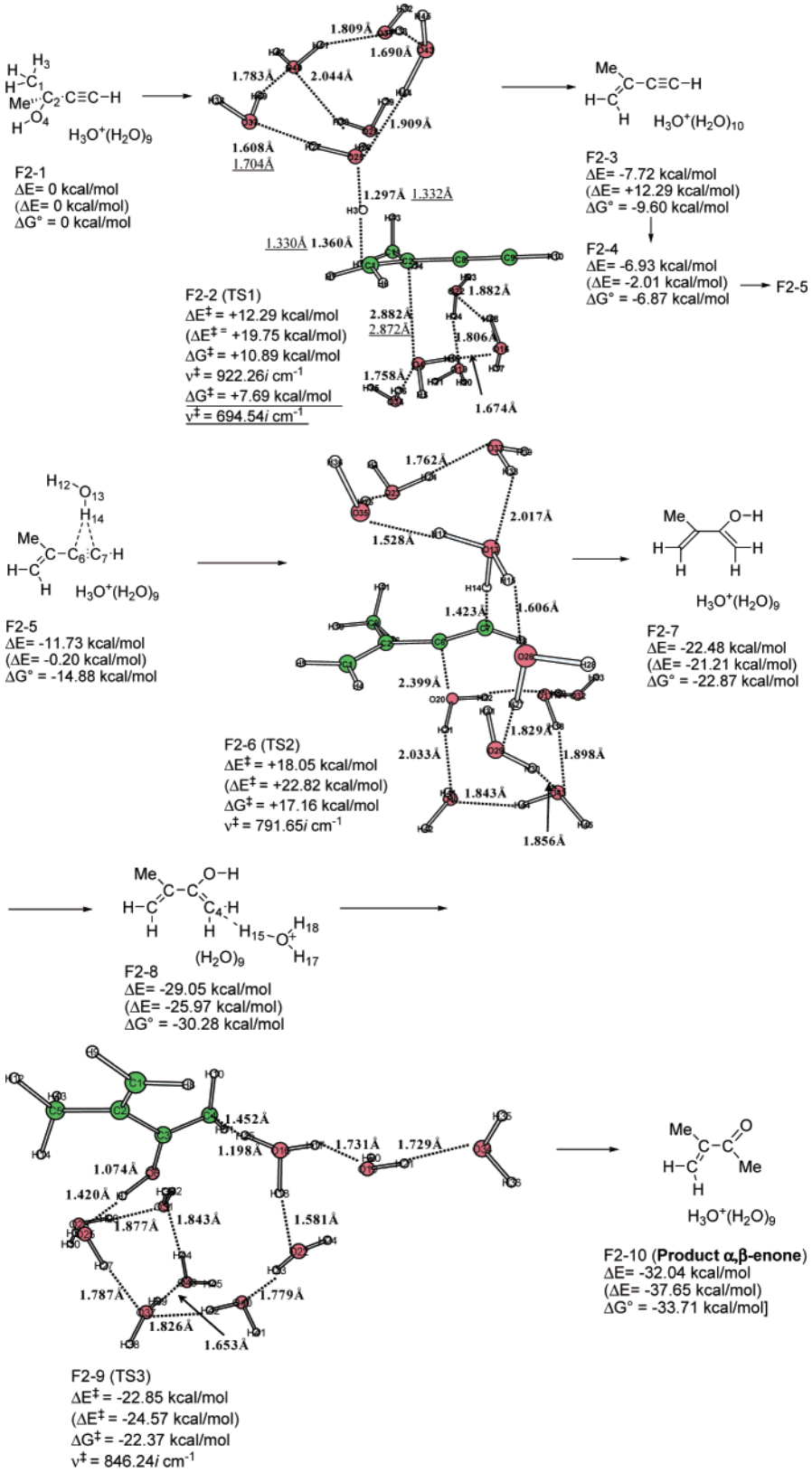

Figure 2. Reaction paths of the Rupe rearrangement by the model in Scheme 5. TS geometries are shown. The reactant, intermediates, and product geometries and reaction-coordinate vectors corresponding to the respective sole imaginary frequencies for TSs are shown in Figure S2 in the Supporting Information. Relative energies (ΔE's) are by RBLYP/6-31G* ZPEs and RB3LYP/6-311+G(d,p) SCRF = dipole electronic energies (without parentheses) and RB3LYP/6-31G* ZPEs and electronic energies (with parentheses). The Gibbs free energy changes are composed of the RB3LYP/6-311+G(d,p) SCRF = dipole electronic energies and RB3LYP/6-31G* thermal corrections to the free energies. The underlined numbers for F-2 (TS1) were obtained by a model excluding three water molecules [7], [8], and [9] in Scheme 5, i.e., $Me_2C(OH)-C\equiv C-H + H_3O^+(H_2O)_6$. F2-1 and F2-2 of the model are shown in Figure S6 (Supporting Information).

Scheme 4. (A) Electrophile $H_3O^+(H_2O)$ Coordinated to the HOMO of the Substrate along the Direction of the Two Arrows and (C) Slight C−O Elongation (1.484 Å in B → 1.684 Å in C) in the Acid-Catalyzed Substrate Providing the LUMO Shape for the Three Reaction Channels

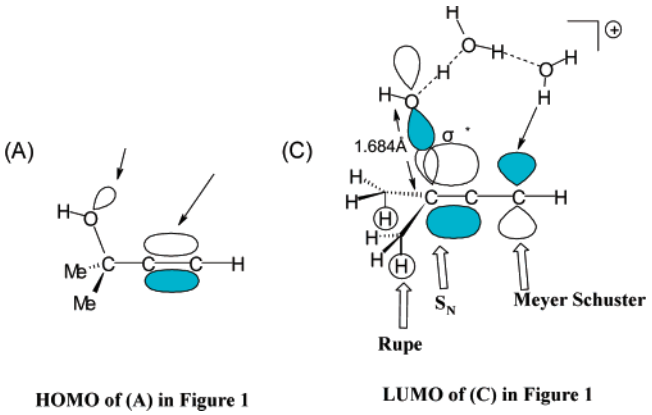

MO of $H_3O^+(H_2O)$, leading to the geometry of Figure 1B. By the coordination, the HOMO and lowest unoccupied molecular orbital (LUMO) energies are lowered considerably, E(HOMO) = −0.32 → −0.49 au and E(LUMO) = +0.38 → +0.19 au. However, LUMO(B) of the complex $Me_2C(OH)-C{\equiv}CH(H_3O)^+H_2O$ is localized at the catalyst part, $-OH\cdots H_3O^+\cdots OH_2$, and does not apparently show the reactivity of the substrate toward the nucleophilic attack by other water molecules. Some distortion from the equilibrium structure (B) would cause the reactivity. To examine the distortion effect, we made a partial geometry optimization of the $H_3O^+(H_2O)$ complexed substrate with the C−O length elongated (1.684 Å) and fixed. At that geometry, LUMO-(C) is depicted and is shown also in Figure 1C. It is noteworthy that, while E[HOMO(C)] = −0.50 au is almost the same as E[HOMO(B)] = −0.49 au, E[LUMO(C)] = +0.09 au is further lowered relative to E[LUMO(B)] = +0.19 au. Besides the enhanced electrophilic character, LUMO(C) has large spatial extensions on three sites of the substrate (Scheme 4).

A nucleophile may attack the sites, leading to three different reaction channels. When a methyl C−H bond is attacked, the Rupe rearrangement is initiated. When the backside of the C−O bond is attacked, a solvolytic S_N (nucleophilic substitution) type displacement occurs. When the acetylenic terminal carbon is attacked, the Meyer−Schuster rearrangement is brought about. According to the

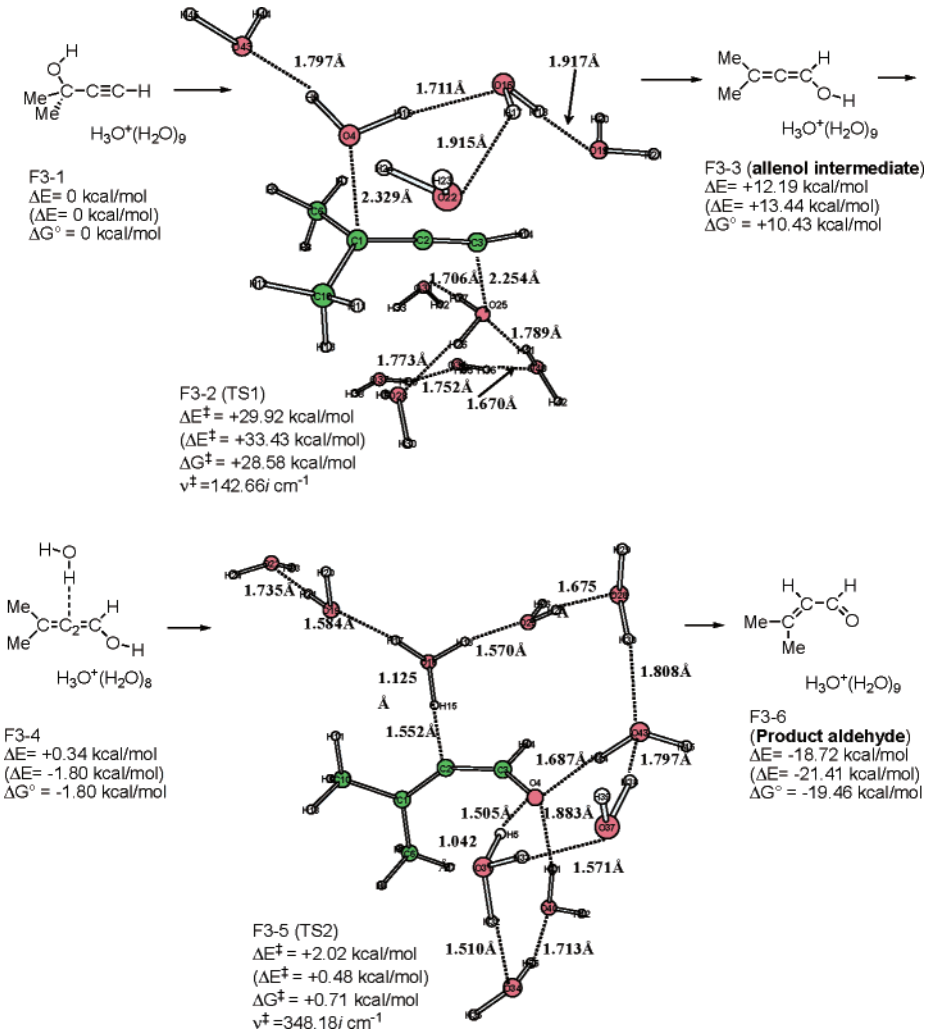

Figure 3. Reaction paths of the Meyer−Schuster rearrangement. TS geometries are shown. The reactant, intermediate, and product geometries and reaction-coordinate vectors corresponding to the respective sole imaginary frequencies for TSs are shown in Figure S3 in the Supporting Information.

Scheme 5. Model of the Rupe Rearrangement to Trace the Reaction Path[a]

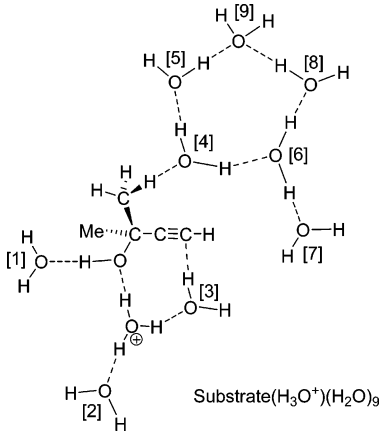

[a] To the nine water molecules the numbers [1], [2], ... [9] are attached for explanation.

LUMO(C) shape, the S_N route needs to also be examined. The S_N product is the same as the substrate with the stereochemical scrambling.

Figure 1 should be reviewed. The acid-catalyzed substrate itself appears not to have a clear reactivity of those reaction channels. But, when the geometry is distorted along the 28th normal-mode vibration, the reactivity is successfully presented (Figure S1 in the Supporting Information). In this regard, the driving force of the two rearrangements is the C−O bond elongation.

Reaction Paths of the Rupe and Meyer−Schuster Rearrangements of $Me_2C(OH)$−C≡C−H. To investigate the role of the proton relay along hydrogen bonds on the Rupe rearrangement, a model, $Me_2C(OH)$−C≡C−H + H_3O^+ + $(H_2O)_9$, was made and is shown in Scheme 5. In the scheme, the first water molecule [1] is linked with the hydroxyl group. [2] and [3] are needed to cover the hydronium ion. Also, [3] is for protonation to the terminal acetylene carbon. Water molecule [4] is the nucleophile (base) to remove the methyl proton. The resultant H_3O^+ must be surrounded by water molecules, which are [5], [6], [8], and [9]. Molecule [7] is added to the model as a potential linkage between H_3O^+[1][2][3] and [4][5][6][8][9].

If more water molecules were added to the model, the calculated results would give more reliable results. However, the model expansion is extremely difficult, because we need to treat the $Ph_2C(OH)$−C≡C−H substrate for the Meyer−Schuster rearrangement with the same solvation pattern. Figure 2 exhibits the reaction path of $Me_2C(OH)$−C≡C−H + H_3O^+ + $(H_2O)_9$ → H_2C=C(Me)−CO−Me + H_3O^+ + $(H_2O)_9$. The geometry of F2-1 is shown in Figure S2 in the Supporting Information and corresponds to that in Scheme 5. The O(25) atom in the $(H_2O)_6$ cluster is a nucleophile (base) to cause the trans elimination (TS1, F2-2).[20] The trans orientation of the E2 reaction is confirmed by the dihedral angle, ∠H3−C1−C2−O4 = −179.04°. At TS1, the C1−H3 and C2−O4 bonds are cleaved at the same time. That is, the carbonium ion does not intervene. The nucleophilicity (basicity) of the $(H_2O)_6$ cluster is strong enough to preclude the carbonium ion and to give a small activation energy, $\Delta E^{\ddagger}$ = +12.29 kcal/mol, in comparison with the average C−H bond energy, 98 kcal/mol. After TS1, the enyne intermediate mediated by the $H_3O^+(H_2O)_{10}$ is formed and is shown in F2-3 (Figure S2 of the Supporting Information). Through the proton transfer along the hydrogen bond, the cation center (i.e., H_3O^+) is moved readily and the isomers of the hydrogen-bond network around the substrate are generated (F2-3, F2-4, and F2-5 shown in Figure S2 of the Supporting Information). In the isomer F2-5, a water molecule (H14O13H12) is bound weakly to the C6≡C7 acetylenic

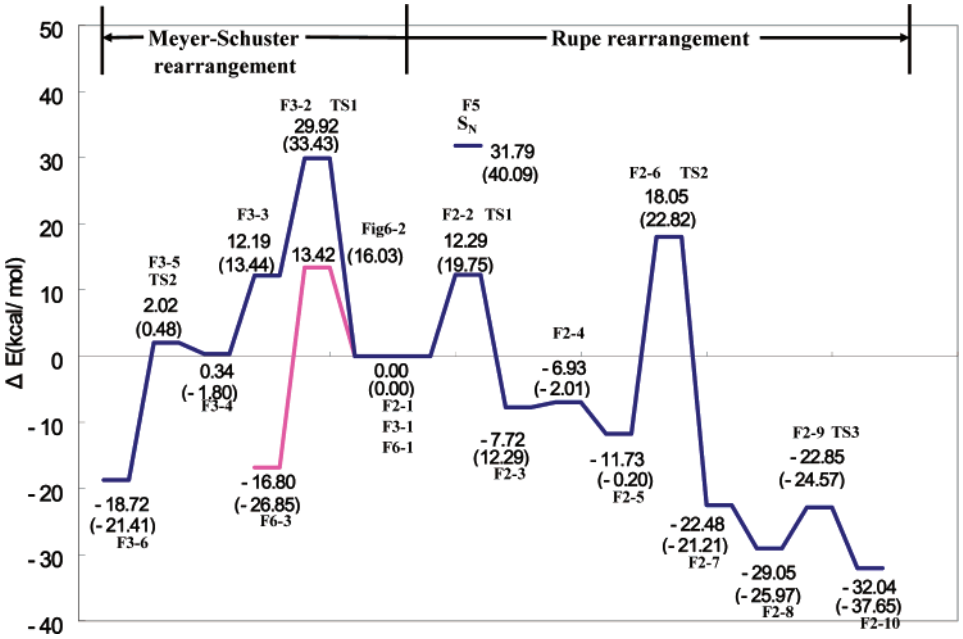

Figure 4. Energy changes for Rupe and Meyer−Schuster rearrangements. Values without parentheses were obtained by the sum of the RB3LYP/6-311+G(d,p) SCRF electronic energy and RB3LYP/6-31G(d) ZPEs. Those with parentheses were obtained by the sum of RB3LYP/6-31G(d) electronic energies and ZPEs. The experimental activation energy of the Meyer−Schuster rearrangement of $Ph_2C(OH)$−C≡C−H is 18.5 kcal/mol.[5]

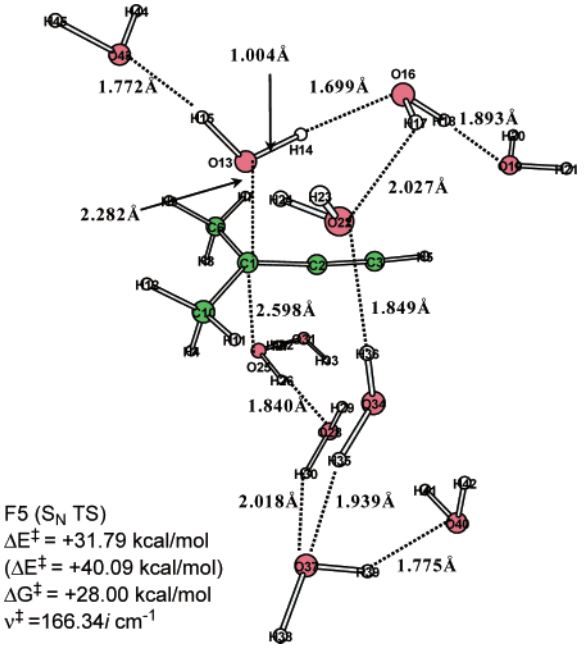

Figure 5. TS geometry of the nucleophilic displacement reaction (S_N) at the C1 center. Reaction-coordinate vectors corresponding to the sole imaginary frequency are shown in Figure S4 in the Supporting Information.

bond (2.344 and 2.211 Å). When a proton (H14) approaches the terminal carbon atom, TS2 (F2-6) is obtained. The C7−H14 and C6−O20 bonds are formed synchronously, leading to a dienal, $H_2C{=}CMe{-}C(OH){=}CH_2$, mediated by H_3O^+-$(H_2O)_9$ (F2-7 in Figure S2 of the Supporting Information). Its isomer is shown in F2-8 (Figure S2), where the hydronium ion H15H18H17(O16)$^+$ is in contact with the terminal vinyl carbon, C4 (1.871 Å). The protonation H15 → C4 and deprotonation O6 → H7 occur simultaneously at TS3 (F2-9). After TS3, the product α,β-enone solvated by H_3O^+-$(H_2O)_9$ (F2-10 in Figure S2 of the Supporting Information) is formed.

Thus, the proton attachment and detachment at the reaction center occur readily in the combination of the dimethylpropargyl alcohol, H_3O^+ and $(H_2O)_9$ cluster. In Scheme 3, the two transition-state models have been shown. The results in Figure 2 basically support the bimolecular dehydration−hydration sequence in the criterion of the hydrogen-bond directionality. There are three transition states: TS1 is the elimination, TS2 is the addition, and TS3 is the isomerization.

Experimentally, the substrate undergoes not the Meyer−Schuster but the Rupe rearrangement. However, the former rearrangement is examined here both to seek its elementary processes and to check whether it is unfavorable relative to the Rupe rearrangement in the present model. Figure 3 exhibits the reaction paths of the Meyer−Schuster rearrangement. The hydrogen-bond chain of the precursor (F3-1 shown in Figure S3, Supporting Information) is slightly different from but practically similar to that in F2-1. At TS1 (F3-2), C1−O4 bond scission and C3−O25 bond formation occur at the same time. Again, no carbonium-ion intermediate is formed. After TS1, an allenol [$Me_2C{=}C{=}CH(OH)$] mediated by $H_3O^+(H_2O)_9$ is obtained, which is shown in F3-3 (Figure S3 of the Supporting Information). Next, the hydrogen-bond chain is reorganized (F3-4 in Figure S3) so that the protonation to the central carbon (C2) of the allenol intermediate is ready. At TS2 (F3-5), protonation (H15 → C2) and deprotonation (O4 → H5) occur simultaneously. After TS2, the product, the α,β-unsaturated aldehyde ($Me_2C{=}CH{-}CHO$) mediated by $H_3O^+(H_2O)_9$, is generated (F3-6 in Figure S3). The dehydration−hydration sequence has been

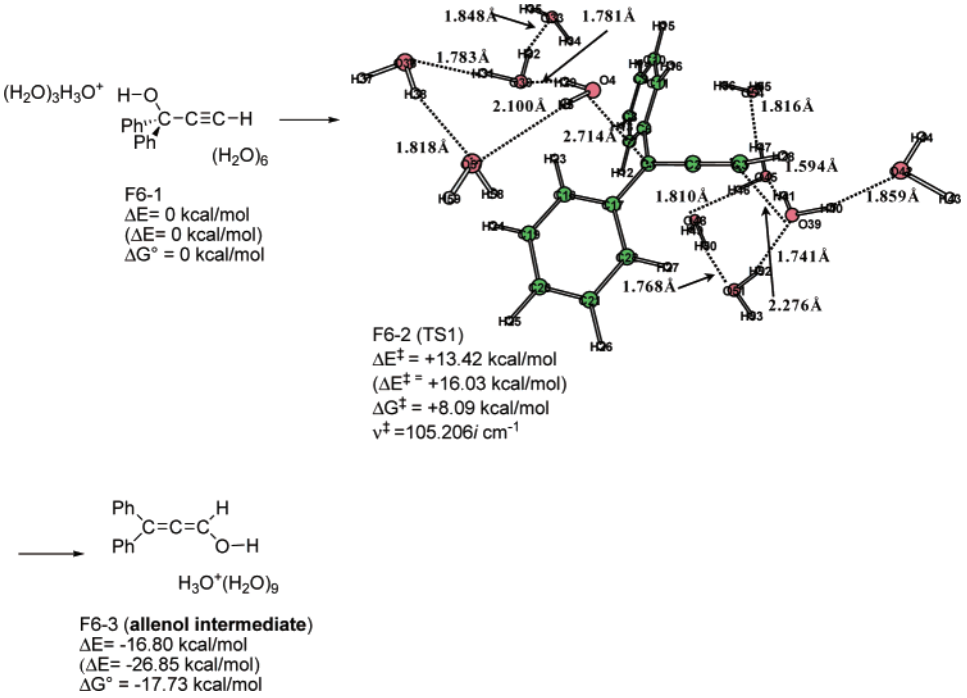

Figure 6. First and rate-determining steps of the Meyer−Schuster rearrangement for the system of $Ph_2C(OH){-}C{\equiv}C{-}H$ + H_3O^+ + $(H_2O)_9$. TS geometry is shown. The reactant and intermediate geometries and reaction-coordinate vectors corresponding to the sole imaginary frequencies for TS1 are shown in Figure S5 in the Supporting Information.

attained by the proton relay through the hydrogen-bond chain, that is, the bimolecular model in Scheme 3.

Figure 4 shows the energy changes (blue color) along both rearrangements. In the Rupe rearrangement, the rate-determining step is TS2, which is consistent with the experimental evidence that the enyne intermediate could be isolated.[4] If TS1 were the rate-determining step, the isolation would be infeasible. On the other hand, the rate-determining step of the Meyer−Schuster rearrangement is TS1. Its activation energy is significantly larger than that of TS2 (Rupe). Therefore, it is found that the reaction channel of the Meyer−Schuster rearrangement is present for the $Me_2C(OH)$−C≡C−H substrate but has a large activation energy and is unlikely.

According to the LUMO(C) extension in Figure 1 and Scheme 4, the S_N path was also investigated. Its TS structure (F5) is shown in Figure 5. It is a carbonium-ion-like structure, which is similar to the TS1s of both rearrangements (with large C−O distances). The TS (S_N) energy is also shown in Figure 4 and is found to be larger even than that of TS1 of the Meyer−Schuster rearrangement. Consequently, although the S_N path is present as predicted in Scheme 4, it has an significantly large activation energy and is unlikely. The stereochemistry of the substrate should be conserved.

Reaction Paths of the Meyer−Schuster Rearrangement of $Ph_2C(OH)$−C≡C−H. The energy diagram in Figure 4 has demonstrated that TS1 is obviously the rate-determining step in the Meyer−Schuster rearrangement. For 1,1-diphenylprop-2-yn-1-ol (R = Ph), accordingly, only the first step was investigated and is shown in Figure 6. The precursor geometry of F6-1 in Figure S5 (Supporting Information) corresponds to that of F3-1 for 2-methylbut-3-yn-2-ol (R = Me). The two hydrogen-bonded water clusters are separated in F6-1, which is in contrast to the linked water clusters in F3-1. The π electron densities on two phenyl groups block the linkage. F6-2 shows TS1 where the C1···O4 bond is to be cleaved (dehydration) and the C3···O39 bond is to be formed (hydration). Noteworthy are their distances, C1···O4 = 2.714 Å and C3···O39 = 2.276 Å. While the latter is close to the corresponding distance, C3···O25 = 2.254 Å (TS1 in F3-2), the former is appreciably larger than C1···O4 = 2.329 Å (TS1 in F3-2). Owing to the extension of the delocalization of the cation charge to the two phenyl rings, TS1 in F6-2 is more carbonium-ion-like than that in F3-2. After TS1, a diphenyl allenol intermediate solvated by $H_3O^+(H_2O)_9$ is formed (F6-3 in Figure S5 of the Supporting Information). In Figure 4, the energy change for the rearrangement of the diphenyl substrate is shown. The calculated activation energy, 13.42 (16.03) kcal/mol, is somewhat smaller than but comparable to the experimental value, 18.5 kcal/mol.[5] The substitution of the methyl group to the phenyl group in the $R_2C(OH)$−C≡C−H substrate lowers the activation energy remarkably, 29.92 (33.43) kcal/mol for R = Me → 13.42 (16.03) for R = Ph. Thus, the condition for the Meyer−Schuster rearrangement is not only the absence of the Rupe-shift C−H bond but also the substituent for the cation charge delocalization.

Scheme 6. Minimal Models to Represent the Reaction Mechanisms[a]

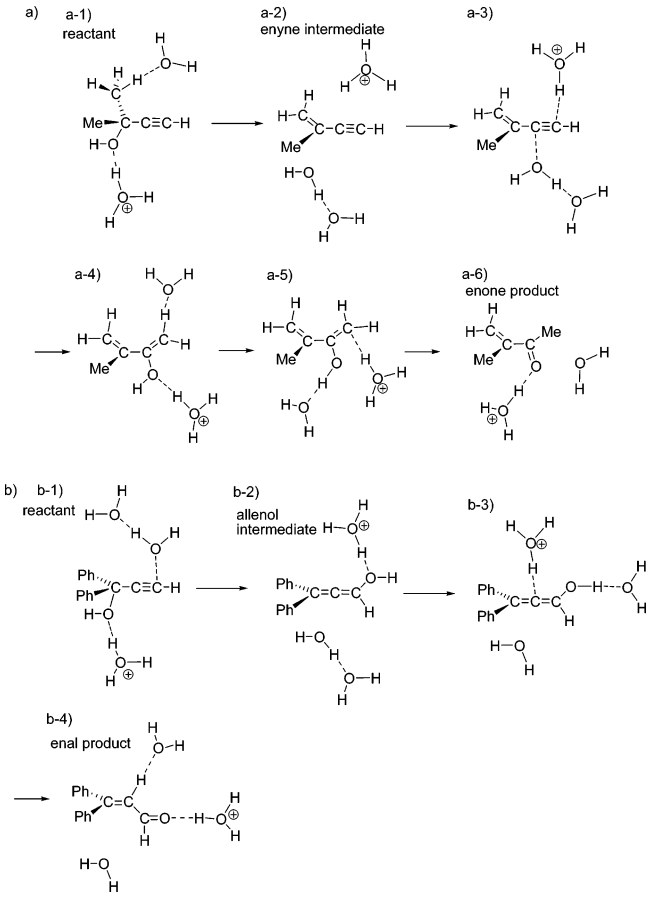

[a] For the Rupe rearrangement, (a) $Me_2C(OH)$−C≡CH + $H_3O^+(H_2O)_1$. For the Meyer−Schuster rearrangement, (b) $Ph_2C(OH)$−C≡CH + $H_3O^+(H_2O)_2$.

IV. Concluding Remarks

In this work, Rupe and Meyer−Schuster rearrangements for the $R_2C(OH)$−C≡C−H + H_3O^+ and $(H_2O)_9$ model have been investigated by the use of RB3LYP calculations. In the substrate $R_2C(OH)$−C≡CH catalyzed by $H_3O^+(H_2O)$, the electrophilic reactivities of the three reaction channels, the two rearrangements and S_N, have been unveiled by the slight C−O bond elongation. The S_N path is unfavorable because the LUMO(C) in Scheme 4 is bonding along the C−C bond (a vague reaction center at the backside of the C−O bond). For the substrate (R = Me), the Rupe rearrangement has been found to be much more favorable than the Meyer−Schuster rearrangement. For the substrate (R = Ph), this shift is very likely with the small activation energy. Both rearrangements do not involve the carbonium-ion intermediates. However, the calculated geometries of TS1 are carbonium-ion-like. Dehydration and hydration may occur via the intermolecular proton relay along the hydrogen-bond chains.

In view of the present calculated results, the reaction mechanism of the two rearrangements may be described by the use of $R_2C(OH)$−C≡C−H and $H_3O^+(H_2O)_n$ (n = 1 in Scheme 6a and n = 2 in Scheme 6b).

In a-1, the substrate is coordinated by H_3O^+ and H_2O. An E2 elimination leads to the enyne intermediate in a-2. The

acetylenic terminal carbon is coordinated by H_3O^+ and the other carbon by $(H_2O)_2$ in a-3. The formation of C−H and C−O bonds gives the enol intermediate in a-4. Its isomerization leads to a-5 and results in the enone product of a-6.

In b-1, the substrate is coordinated by H_3O^+ and $(H_2O)_2$. The C−O bond cleavage and formation leads to an allenol intermediate in b-2. The allenic center carbon atom and the hydroxy proton of the intermediate are coordinated by H_3O^+ and H_2O, respectively, in b-3. Protonation and deprotonation give the enal product in b-4. Thus, the Rupe and Meyer−Schuster rearrangements are composed of protonation, deprotonation, C−O bond cleavage, and its formation. The $H_3O^+(H_2O)_n$, $n = 1$ for a or $n = 2$ for b, species may describe the bond interchanges in the minimal sizes. Bond interchanges along hydrogen bonds work effectively to cause both rearrangements.

Supporting Information Available: The 28th normal-mode vibration of $Me_2C(OH)C{\equiv}CH$ with $H_3O^+(H_2O)$ (Figure S1) and reactant, intermediate, and product geometries and reaction-coordinate vectors corresponding to respective sole imaginary frequencies for TSs (Figures S2−S6). This material is available free of charge via the Internet at http://pubs.acs.org.

References

(1) (a) Rupe, H.; Glenz, K. *Liebigs Ann. Chem*. **1924**, *436*, 184−204. (b) Rupe, H.; Kambli, E. *Helv. Chim. Acta* **1926**, *9*, 672. (c) Rupe, H.; Kambli, E. *Liebigs Ann. Chem*. **1927**, *459*, 195−217. (d) Rupe, H.; Giesler, L. *Helv. Chim. Acta* **1928**, *11*, 656−669. (e) Rupe, H.; Messner, W.; Kambli, E. *Helv. Chim. Acta* **1928**, *11*, 449−462. (f) Rupe, H.; Wirz, A.; Lotter, P. *Helv. Chim. Acta* **1928**, *11*, 965−971. (g) Rupe, H.; Gassmann, A. *Helv. Chim. Acta* **1929**, *12*, 193−204. (h) Rupe, H.; Hirschmann, H. *Helv. Chim. Acta* **1931**, *14*, 687−701. (i) Rupe, H.; Kuenzy, F. *Helv. Chim. Acta* **1931**, *14*, 701−708. (j) Rupe, H.; Kuenzy, F. *Helv. Chim. Acta* **1931**, *14*, 708−718. (k) Rupe, H.; Haecker, R.; Kambli, E.; Wassieleff, N. *Helv. Chim. Acta* **1933**, *16*, 685−700. (l) Rupe, H.; Gassmann, A. *Helv. Chim. Acta* **1934**, *17*, 283−285. (m) Rupe, H.; Werdenberg, H. *Helv. Chim. Acta* **1935**, *18*, 542−546.

(2) Meyer, K. H.; Schuster, K. *Chem. Ber*. **1922**, *55*, 819−823.

(3) Swaminathan, S.; Narayanan, K. V. *Chem. Rev*. **1971**, *71*, 429−438.

(4) (a) Hurd, C. D.; Jones, R. N. *J. Am. Chem. Soc*. **1934**, *56*, 1924−1926. (b) Ansell, M. F.; Hancock, J. W.; Hickinbottom, W. J. *J. Chem. Soc*. **1956**, 911−917. (c) Coles, L. E.; Linnell, W. H.; Mathieson, D. W.; Shoukri, A. S. *J. Chem. Soc*. **1954**, 2617−2622. (d) Hamlet, J. C.; Henbest, H. B.; Jones, E. R. H. *J. Chem. Soc*. **1951**, 2652−2659. (e) Inhoffen, H. H.; Longemann, W.; Hohlweg, W.; Serini, A. *Chem. Ber*. **1938**, *71*, 1024−1032. (f) Smissmann, E. E.; Johnson, R. H.; Carlson, A. W.; Aycock, B. F. *J. Am. Chem. Soc*. **1956**, *78*, 3395−3400.

(5) Edens, M.; Boerner, D.; Chase, C. R.; Nase, D.; Schiavelli, M. D. *J. Org. Chem*. **1977**, *42*, 3403−3408.

(6) Stevens, K. E.; Paquette, L. A. *Tetrahedron Lett*. **1981**, *22*, 4393−4396.

(7) Takeda, K.; Nakane, D.; Takeda, M. *Org. Lett*. **2000**, *2*, 1903−1905.

(8) Weinmann, H.; Harre, M.; Neh, H.; Nickisch, K.; Skötsch, C.; Tilstam, U. *Org. Process Res. Dev*. **2002**, *6*, 216−219.

(9) Stark, H.; Sadek, B.; Krause, M.; Hüls, A.; Ligneau, X.; Ganellin, C. R.; Arrang, J.-M.; Schwartz, J.-C.; Schunack. W. *J. Med. Chem*. **2000**, *43*, 3987−3994.

(10) Welch, S. C.; Hagan, C. P.; White, D. H.; Fleming, W. P.; Trotter, J. W. *J. Am. Chem. Soc*. **1977**, *99*, 549−556.

(11) Yoshimatsu, M.; Naito, M.; Kawahigashi, M.; Shimizu, H.; Kataoka, T. *J. Org. Chem*. **1995**, *60*, 4798−4802.

(12) An, J.; Bagnell, L.; Cablewski, T.; Strauss, C. R.; Trainor, R. W. *J. Org. Chem*. **1997**, *62*, 2505−2511.

(13) (a) Imagawa, H.; Asai, Y.; Takano, H.; Hamagaki, H.; Nishizawa, M. *Org. Lett*. **2006**, *8*, 447−450. (b) Narasaka, K.; Kusama, H.; Hayashi, Y. *Chem. Lett*. **1991**, 1413−1416. (c) Narasaka, K.; Kusama, H.; Hayashi, Y. *Tetrahedron* **1992**, *48*, 2059−2068. (d) Lorber, C. Y.; Osborn, J. A. *Tetrahedron Lett*. **1996**, *37*, 853−856. (e) Chabardes, P. *Tetrahedron Lett*. **1988**, *29*, 6253−6256. (f) Suzuki, T.; Tokunaga, M.; Wakatsuki, Y. *Tetrahedron Lett*. **2002**, *43*, 7531−7533. (g) Mercier, C.; Chabardes, P. *Pure Appl. Chem*. **1994**, *66*, 1509−1518. (i) Cadierno, V.; Diez, J.; Garcia-Garrido, S. E.; Gimeno, J. *Chem. Commun*. **2004**, 2716−2717.

(14) (a) Bigi, F.; Carloni, S.; Maggi, R.; Muchetti, C.; Sartori, G. *J. Org. Chem*. **1997**, *62*, 7024−7027. (b) Luzung, M. R.; Tosle, F. D. *J. Am. Chem. Soc*. **2003**, *125*, 15760−15761. (c) Ishikawa, T.; Manabe, S.; Aikawa, T.; Kudo, T.; Saito, S. *Org. Lett*. **2004**, *6*, 2361−2364. (d) Zhao, W.; Carreira, E. M. *Org. Lett*. **2003**, *5*, 4153−4154.

(15) (a) Tapia, O.; Lluch, J. M.; Cardenas, R.; Andres, J. *J. Am. Chem. Soc*. **1989**, *111*, 829−835. (b) Andres, J.; Cardenas, R.; Silla, E.; Tapia, O. *J. Am. Chem. Soc*. **1988**, *110*, 666−674. (c) Andres, J.; Silla, E.; Tapia, O. *J. Mol. Struct*. **1986**, *138*, 171−177. (d) Tapia, O.; Andres, J. *Chem. Phys. Lett*. **1984**, *109*, 471−477. (e) Andres, J.; Silla, E.; Tapia, O. *Chem. Phys. Lett*. **1983**, *94*, 193−197. (f) Andres, J.; Silla, E.; Tapia, O. *J. Mol. Struct*. **1983**, *105*, 307−314.

(16) (a) Becke, A. D. *J. Chem. Phys*. **1993**, *98*, 5648−5652. (b) Lee, C.; Yang, W.; Parr, R. G. *Phys. Rev. B* **1988**, *37*, 785−789.

(17) (a) Fukui, K. *J. Phys. Chem*. **1970**, *74*, 4161−4163. (b) Gonzalez, C.; Schlegel, H. B. *J. Phys. Chem*. **1990**, *94*, 5523−5527.

(18) (a) Onsager, L. *J. Am. Chem. Soc*. **1936**, *58*, 1486-1493. (b) Tapia, O.; Goscinski, O. *Mol. Phys*. **1975**, *29*, 1653−1661.

(19) Frisch, M. J.; Trucks, G. W.; Schlegel, H. B.; Scuseria, G. E.; Robb, M. A.; Cheeseman, J. R.; Montgomery, J. A., Jr.; Vreven, T.; Kudin, K. N.; Burant, J. C.; Millam, J. M.; Iyengar, S. S.; Tomasi, J.; Barone, V.; Mennucci, B.; Cossi, M.; Scalmani, G.; Rega, N.; Petersson, G. A.; Nakatsuji, H.; Hada, M.; Ehara, M.; Toyota, K.; Fukuda, R.; Hasegawa, J.; Ishida, M.; Nakajima, T.; Honda, Y.; Kitao, O.; Nakai, H.; Klene, M.; Li, X.; Knox, J. E.; Hratchian, H. P.; Cross, J. B.; Adamo, C.; Jaramillo, J.; Gomperts, R.; Stratmann, R. E.; Yazyev, O.; Austin, A. J.; Cammi, R.; Pomelli, C.; Ochterski, J. W.; Ayala, P. Y.; Morokuma, K.; Voth, G. A.; Salvador, P.; Dannenberg, J. J.; Zakrzewski, V. G.; Dapprich, S.; Daniels, A. D.; Strain, M. C.; Farkas, O.; Malick, D. K.; Rabuck, A. D.; Raghavachari, K.; Foresman, J. B.; Ortiz, J. V.; Cui, Q.; Baboul, A. G.; Clifford, S.; Cioslowski, J.; Stefanov, B. B.; Liu, G.; Liashenko, A.; Piskorz, P.; Komaromi, I.; Martin, R. L.; Fox, D. J.; Keith, T.; Al-Laham, M. A.; Peng, C. Y.; Nanayakkara, A.; Challacombe, M.; Gill, P. M. W.; Johnson, B.; Chen, W.; Wong, M. W.; Gonzalez, C.; Pople, J. A. *Gaussian 03*, revision C.02; Gaussian, Inc.: Pittsburgh, PA, 2003.

(20) The TS1 geometry of the substrate$-H_3O^+(H_2O)_6$ system was also calculated. In the system, three water molecules [7], [8], and [9] in Scheme 5 were excluded. The underlined numbers for the system are similar to those for the substrate$-H_3O^+(H_2O)_9$. Data of TS1 (F2-2) and the precursor (F2-1) of the $H_3O^+(H_2O)_6$ system are shown in Figure S6 (Supporting Information).

CT600132K